Rotor Design for Whirl Flutter: An Examination of Options for Improving Tiltrotor Aeroelastic Stability Margins

C. W. Acree, Jr.
Aerospace Engineer
NASA Ames Research Center

R. J. Peyran
Aerospace Engineer
U.S. Army Aeroflightdynamics Directorate

Wayne Johnson
Aerospace Engineer
NASA Ames Research Center

Abstract

Rotor design changes intended to improve tiltrotor whirl-flutter stability margins were analyzed. A baseline analytical model similar to the XV-15 (23% thick wing) was established, and then a 15% thick wing design was developed. A simplified finite-element model of the airframe was used for the structural design. This thinner wing is representative of a wing for a high-speed tiltrotor with good aerodynamic performance. While it has lower drag, it also has lower stiffness, reducing the flight speed for whirl-flutter instability. Changes to the rotor blade design were investigated with the objective of increasing the stability speed margin for this thin-wing design. Small rearward offsets of the aerodynamic center with respect to the blade elastic axis and pitch axis created large increases in the stability boundary. The effect was strongest for offsets at the outboard part of the blade, where an offset of 10% of tip chord improved the stability margin by over 100 knots. Forward offsets of the blade center of gravity had similar but less pronounced effects. A limited investigation of blade loads in helicopter and airplane configuration indicated that proper choice of parametric variations can avoid excessive increases in rotor loads.

Notation

AC	blade chordwise aerodynamic center, positive aft
CG	blade chordwise center of gravity, positive forward
C_T/σ	thrust coefficient, divided by solidity
R	rotor radius
t/c	wing thickness-to-chord ratio
Δ	change in blade chordwise AC or CG position
μ	advance ratio

Introduction

Coupled wing/rotor whirl-mode aeroelastic instability is the major barrier to increasing tiltrotor speeds. Increased power, thrust, and rotor efficiency are of no avail unless the whirl-mode stability boundary can be improved. With current technology, very stiff, thick wings of limited aspect ratio are essential to meet the stability requirements, which severely limits cruise efficiency and maximum speed.

Numerous approaches to improving the whirl-mode boundary have been investigated, including tailored stiffness wings (Refs. 1-3), active stability augmentation (Ref. 4), variable geometry rotors (Ref. 5), highly swept tips (Ref. 6), and at one extreme, folding rotors (Ref. 7). The research reported herein investigated the much simpler approach of adjusting the chordwise positions of the rotor blade aerodynamic center and center of gravity.

This report discusses first the background to the research, which began with a small model constructed to facilitate rapid rotor design changes. A CAMRAD II analytical model is described, including a matrix of parametric variations of the rotor design. The design and analysis of a new, reduced-thickness wing are discussed in the Appendix. A summary of results for all parametric variations is presented, followed by a few detailed examples. The effects on blade loads are also summarized.

Background

The research began with a very simple, unpowered, table-top model of a wing and rotor (Fig. 1), built of balsa wood and driven by an ordinary box fan. The wing was a ladder-frame structure with no aerodynamic shell, and the rotor was a two-bladed, teetering design. This was the simplest design

Presented at the American Helicopter Society 55th Annual Forum, Montréal, Quebec, Canada, May 25-27, 1999.

possible for testing whirl flutter. The 17-in diameter rotor had a weight extended ahead of the leading edge of each tip. Adjusting the chordwise weight position produced dramatic improvements in whirl-mode stability (Ref. 8).

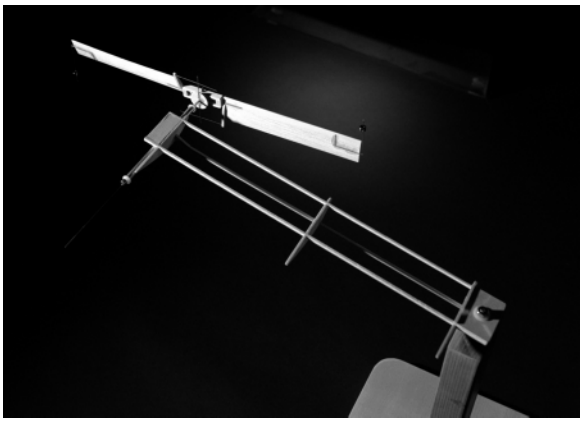

Fig. 1. Table-top tiltrotor whirl-flutter model with tip weights.

Although hardly rigorous, the results were compelling and led immediately to analyses with CAMRAD II (Ref. 9). A semi-span analytical model of the XV-15 confirmed the results of the table-top model. The analytical model and its developments reported here have roots in earlier work reported in Ref. 10.

In classic flutter theory, the distance between the center of gravity and the aerodynamic center is a key parameter. This suggested that moving the aerodynamic center aft should have similar effects to moving the center of gravity forward. The CAMRAD II model was accordingly extended to examine an aerodynamic offset, but near the root of the blade instead of the tip. The aerodynamic offset improved whirl-mode stability, confirming the hypothesis.

Because the semi-span CAMRAD II model could not analyze antisymmetric wing modes, a full-span CAMRAD II model was developed. The semi-span and full-span models both simulated a reduced-thickness wing by arbitrarily lowering the wing structural frequencies. Each model was used to examine the effects of aerodynamic-center offsets along the inboard portion of the blade span and of a tip mass extended forward of the leading edge. Favorable results led directly to the more systematic efforts reported herein.

Analytical Model

A CAMRAD II model of a notional tiltrotor was developed to serve as a baseline for parametric variations of rotor design parameters. The new model was based closely on an existing model of the XV-15, chosen because it is well-proven for stability predictions and thoroughly understood by the authors. See Refs. 10 and 11 for correlation of CAMRAD predictions with measured stability and loads.

Figure 2 is a three-view of the XV-15 with pertinent dimensional data; the moderate aspect ratio of the thick wing is clearly evident. (Detailed specifications are given in Ref. 12.) The model was altered in several ways from the original representation of the XV-15, including a different wing, a simplified drive train, and deletion of wing aerodynamic damping. The new wing model is discussed in detail below. The other changes were made to prevent confounding the effects of rotor parametric variations with the effects of drive-train modes and wing aerodynamic damping.

Airframe

Considerable effort was put into creating a thin, high-speed wing design that could be rigorously compared to the actual XV-15 wing. The new wing has the same geometry as the XV-15 wing, but with a thickness-to-chord ratio (*t/c*) of 15%, a value typical of current commuter aircraft, instead of 23%. Airframe drag was arbitrarily reduced by 25% to simulate the improved aerodynamics expected from a thinner wing.

To calculate aeroelastic stability, CAMRAD II couples externally generated wing modes to internally generated rotor modes. Merely lowering the wing frequencies, as was done in the preliminary research, does not result in mode shapes realistic for a thinner wing. The new wing was modeled in NASTRAN (Ref. 13) to get modal data for input into CAMRAD II. The design and validation of the new wing model are documented in the Appendix.

The XV-15 airframe model evolved through three stages. Details are given in the Appendix; a brief summary is given here. The original CAMRAD II model utilized wing mode shapes and frequencies generated by a detailed NASTRAN model. The second model used NASTRAN data from a much simpler “stick” model of the original, 23% *t/c* wing; this is denoted the “thick wing” model. The third model, used in this study as a baseline reference, used NASTRAN data from a stick model of a 15% *t/c* wing; this is denoted the “thin wing” model. The two NASTRAN stick models differed only in the parameters affected by wing thickness, thereby ensuring

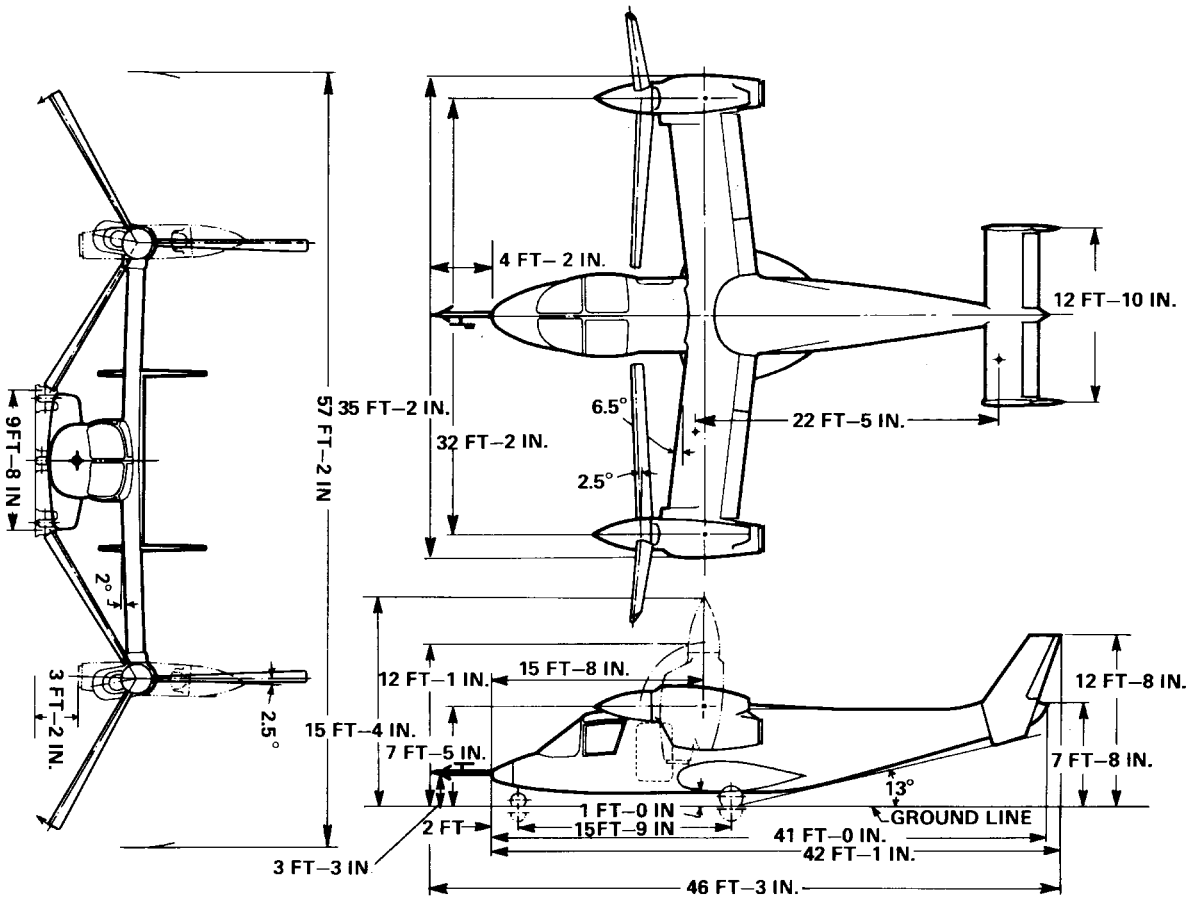

Fig. 2. XV-15 tiltrotor aircraft geometry, with 23% *t/c* wing (Ref. 12).

that comparisions between the thick and thin wings were not confounded by differences in NASTRAN modelling methods.

The primary purpose of the thinner wing, at least as it applies to the present research, is to lower the whirl-mode stability boundary to better reveal the effects of parametric variations of the rotor. Because the rotor was not redesigned for higher speeds, the thin wing is of limited value for increasing cruise performance. Nevertheless, the new wing provides an adequate baseline, so the notional model was not further optimized.

Rotor

The baseline rotor used in the study was the original XV-15 steel-blade rotor, with a 2.5-deg precone titanium hub. This is a rigid (stiff-in-plane) rotor with a gimbaled hub. The inboard aerodynamic sections start with a 17-in chord at 12% radius, linearly tapering to a 14-in chord at 25% radius; the chord is constant from there to the tip (Fig. 3). Total effective blade twist is 45 deg over a 150-in radius (Ref. 14).

The rotor parametric variations were distributed among four radial segments, numbered 1 to 4 from root to tip as shown in Fig. 3. The aerodynamic center (AC) was offset aft in five increments of 5% of tip chord. (Local chord was not used, lest the inboard taper confound the results by creating an effective forward sweep along part of segment #1).

The AC shifts were effected by moving the airfoil quarter-chord aft with respect to the pitch axis, which in this model is the same as the blade elastic axis. The center of gravity (CG) was offset forward in increments of 5% tip chord to match the magnitudes of the AC offsets. The maximum offset was therefore 25% chord, which placed the CG at the leading edge. The two types of offset were analyzed separately. There were thus five discrete values of two parameters each, at four separate radial segments, making a matrix of 40 variations in addition to the baseline.

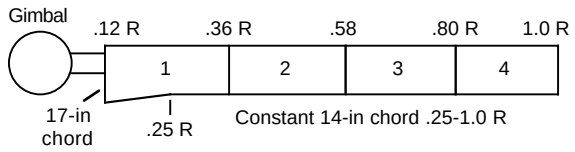

Fig. 3. XV-15 rotor blade planform (untwisted).

Aerodynamic and mass offsets are conceptually similar, in that they both increase the chordwise distance between the center of gravity and aerodynamic center. This is the classic means of increasing flutter stability of an isolated airfoil. Because of the highly coupled nature of whirl-mode instability, it also increases the stability of the entire rotor-wing dynamic system. However, the effects of aerodynamic offset are much stronger than those of mass offset, and the effects on loads are different, as will be shown.

Trim Criteria

Four different trim conditions were considered:

1. Level flight with unlimited power
2. Constant power (climb and dive to match power)
3. Zero power
4. Limited power (level flight up to maximum power, constant power thereafter)

The first is physically unrealistic, and the second is unrepresentative of actual flight operations. The third, zero power, is a special case of constant power, and is a possible emergency flight condition (engine out). The fourth represents normal flight-test operations, wherein the aircraft is trimmed to level flight up to the power- or torque-limited airspeed, then allowed to descend as necessary to achieve the desired airspeed at the torque limit. Here a torque limit of 130,000 in-lb was used, reached at 275 knots with the thin wing.

Limited-power trim usually determines the whirl-mode stability boundary, but for some rotors, zero-power trim is the limiting condition, so both must be examined. For this research, limited-power trim always had a lower instability airspeed than zero power, although not by a large margin. Results for only the former are reported herein.

The rotor was trimmed to 457 rpm (76% of hover design rpm), at sea-level standard conditions. This is the original design cruise rotor speed and not representative of currrent XV-15 operations; it was chosen because it is a nominal design point and highlights the effects of the parametric variations. The speed range was 150 to 400 knots true airspeed, with trim and stability calculated in 25-knot increments.

One further aspect of the trim criteria should be mentioned. Obtaining reliable convergence of the CAMRAD II model at high speeds proved difficult, which is not surprising given that the system was often unstable. CAMRAD II can use different rotor models for trim and stability, and this was exploited differently for the AC-offset cases than for the CG-offset cases. The former converged adequately when the rotor was trimmed with first-harmonic flapping allowed, which simulated a rigid, gimbaled rotor. However, the mass-offset cases were trimmed using only the mean blade motion. A check of the baseline model revealed only very minor differences in the stability predictions for the two different trim models.

For both trim models, hence all cases analyzed, the aeroelastic stability analyses used a rotor model with a gimbal, two degrees of freedom for flap/lag modes and one degree of freedom for torsion modes. The left-right symmetry of the XV-15 was exploited by calculating symmetric and antisymmetric modes separately.

Stability Predictions

Adding up the cases discussed above, there are 11 airspeeds for both trim criteria (zero power and limited power), applied to each of the 40 parametric variations, plus the thick- and thin-wing XV-15 models with the unmodified rotor, for a total of 924 cases. It is practical to present only a general overall summary and a few specific examples.

Baseline Checks

Figures 4 and 5 compare the CAMRAD II predictions for thick- and thin-wing XV-15 whirl modes, plotted as frequency and damping versus airspeed for each of the wing modes. (The thick-wing and thin-wing NASTRAN models are discussed in the Appendix). The intersections of the individual damping curves with the zero-damping axis define the stability boundaries for each mode; the overall whirl-flutter boundary is of course that of the least stable mode.

There are six wing modes to be examined: beamwise bending, chordwise bending, and torsion, each in symmetric (Figs. 4a and 5a) and antisymmetric (Figs. 4b and 5b) forms (see the Appendix for further details). The “beam,” “chord” and “torsion” labels are somewhat arbitrary because of the highly-coupled nature of whirl-mode instabilities.

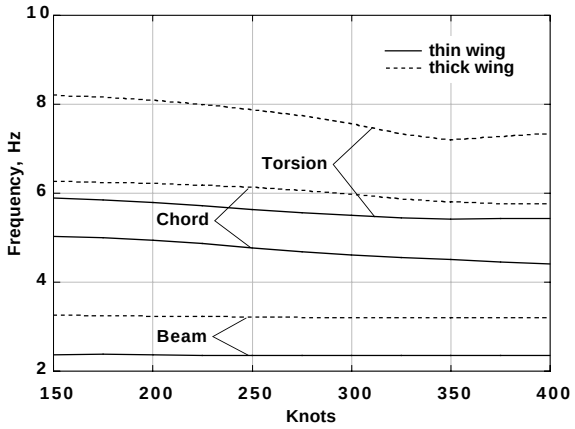

Fig. 4a. Symmetric whirl-mode frequency versus airspeed for the thick- and thin-wing models (457 rpm, sea level).

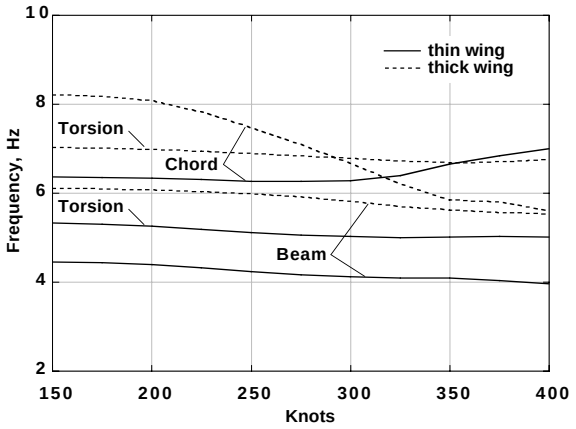

Fig. 4b. Antisymmetric whirl-mode frequency versus airspeed for the thick- and thin-wing models (457 rpm, sea level).

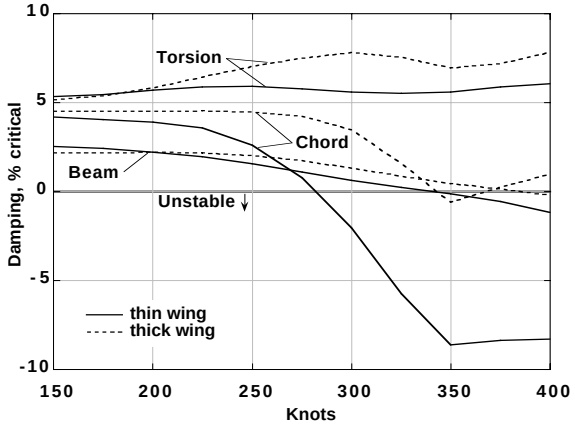

Fig. 5a. Symmetric whirl-mode damping versus airspeed for the thick- and thin-wing models (457 rpm, sea level).

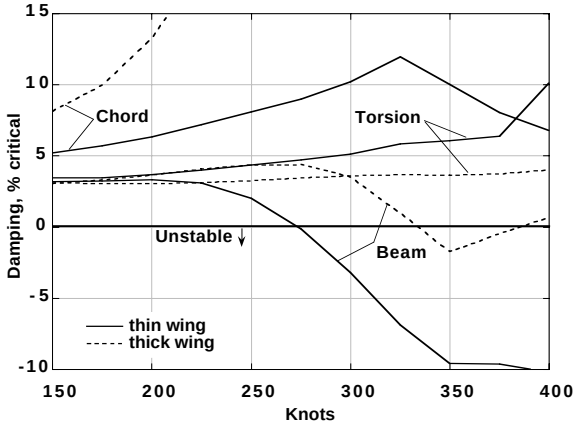

Fig. 5b. Antisymmetric whirl-mode damping versus airspeed for the thick- and thin-wing models (457 rpm, sea level).

Figure 5 clearly shows that symmetric chord and antisymmetric beam are the limiting modes for both the thick- and thin-wing models. It also shows that reducing the wing thickness greatly reduced the symmetric chord, antisymmetric beam, and anti-symmetric chord damping. The other modes were little affected, especially symmetric beam. The stability boundary of the thin-wing model was barely 275 knots, a reduction of 60 knots below that of the original, thick wing. The key point is that the instability airspeed was greatly reduced without changing the basic nature of the limiting modes.

At 400 knots, the tip Mach number is 0.82, placing the tip airfoil section inside the transonic regime. The blade section lift curve slope is decreasing at that point, which improves stability. This effect can be clearly seen in several of the modes in Fig. 5, most notably symmetric chord (Fig. 5a) and antisymmetric beam and torsion (Fig. 5b).

Summary of Parametric Variations

Figures 6 and 7 summarize the changes to the overall stability boundary caused by the variations in AC and CG offsets, which were applied to the thin-wing model. The limiting airspeed was interpolated to the nearest 5 knots for each value of offset (Figs. 6 and 7, respectively). The lower limit of each plot is 275 knots, the stability boundary for the thin wing model with the unmodified rotor. The stability boundary of the modified rotor never dropped below this speed. The upper limit of 400 knots is the maximum speed analyzed.

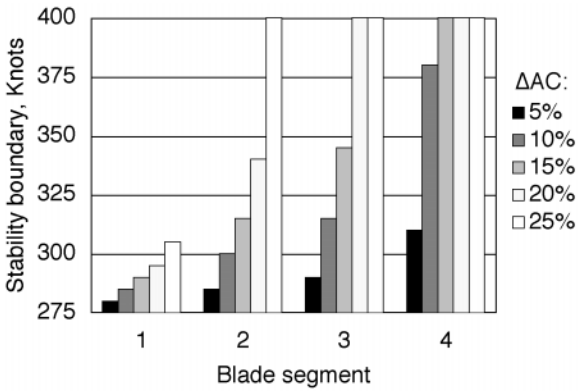

Fig. 6. Whirl-mode stability boundaries for aerodynamic-center offsets, thin-wing model.

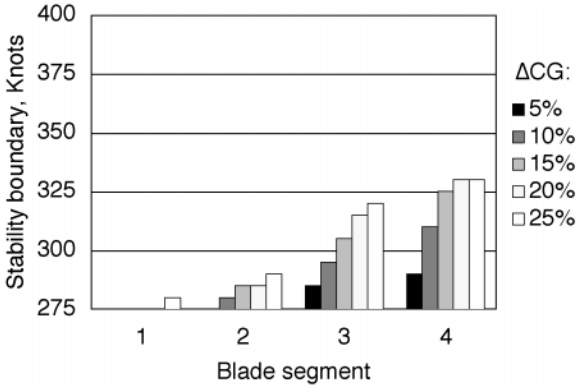

Fig. 7. Whirl-mode stability boundaries for center-of-gravity offsets, thin-wing model.

Eleven of the 40 AC and CG variations increased the instability airspeed by 60 knots or more, which at a minimum fully recovered the stability boundary of the original XV-15 model.

It is immediately apparent that AC offsets are much more effective than CG offsets: usually at least twice as much so (compare Fig. 6 to Fig. 7). Offsets at the tip are more effective than at the root for both types of offset.

For AC offsets, the limiting mode was usually antisymmetric beam, except for the 10% aft AC offset at segment #2, for which the symmetric beam mode determined the instability airspeed.

For CG offsets, the limiting mode was also usually the antisymmetric beam mode. The three exceptions were 25% forward CG offset at segments #3 and #4, and 20% forward CG offset at segment #4, for which the symmetric beam mode was the limiting mode.

The effects of AC offsets were more pronounced than expected. The 400-knot limit of this study prevented a complete evaluation of the ultimate effectiveness of AC and CG offsets at very high speeds, but exploitation of large stability improvements would require a reoptimized rotor. A 400-knot-class proprotor would have different airfoils, twist and planform, and would therefore be expected to show different sensitivities to the parametric variations considered here.

The sensitivity of modal stability to the amount of AC and CG offset is revealed in more detail when the data are plotted for a single blade segment and fixed airspeed. Figures 8 and 9 present damping versus AC and CG offsets, respectively, for blade segment #4 at 350 knots. The outermost blade segment was chosen because the effects are most pronounced for that radial location. An airspeed of 350 knots was chosen because it is high enough to be strongly sensitive to both types of offset, yet not so high as to confound the results with transonic airfoil effects.

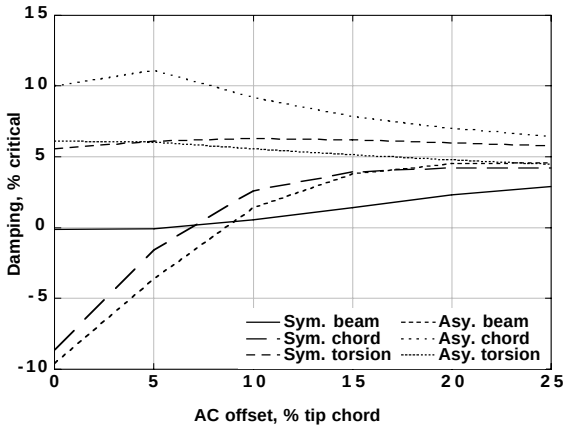

Fig. 8. Variation of damping with aerodynamic-center offset for blade segment #4 at 350 knots.

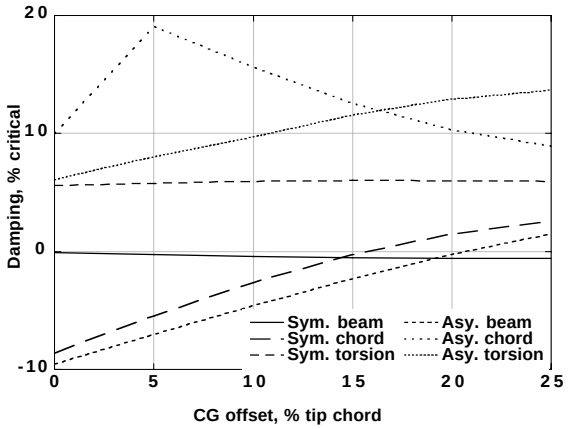

Fig. 9. Variation of damping with center-of-gravity offset for blade segment #4 at 350 knots.

Comparing Fig. 8 to Fig. 9, shifting the aerodynamic center was much more effective than shifting the center of gravity, but only for offsets less than about 10% of tip chord. Increasing the AC offset had almost no effect beyond 15%, while CG offset was effective to the limit of the analysis, although beginning to be less so at 25% offset.

For both types of offset, the wing modes most strongly affected were symmetric chord and anti-symmetric beam. These are the critical modes because they are the least stable at zero offset. At a large enough value of either AC or CG offset, the damping of these two modes becomes greater than the damping of the symmetric beam mode, which is not strongly affected by either AC or CG offsets. However, this analysis included no wing aero-dynamic damping, which would raise the damping of the symmetric beam mode more than any other mode. Therefore, definitive conclusions cannot be drawn from Figs. 8 or 9 concerning the optimum values of AC or CG offset.

Antisymmetric torsion was strongly influenced by CG offsets, but only slightly so by AC offsets. Antisymmetric chord was very sensitive to both offsets, and was the only mode that decreased significantly with either type of offset. Because the damping of both of these modes is already high at zero offset, the variations shown here are of little consequence. Antisymmetric chord damping shows the peculiar behavior of a large increase for a small amount of offset, then a gradual decrease with increasing of offset; the effect is stronger for CG offsets (Fig. 9) than for AC offsets (Fig. 8). This is apparently caused by a strong interaction between wing and rotor modes, such that a small offset of either type significantly separates the modes, resulting in a large change in damping. Once the modes are separated, further changes in offset have much less effect and are of opposite sign. The reader is reminded that mode labels are somewhat arbitrary because of these and other coupling effects. The modes shown here were tracked by frequency, not damping, which partially accounts for the change in slope of the damping.

Figure 8 helps to explain an anomaly noted above for Fig. 6, wherein the limiting mode was the symmetric chord mode in all cases but one: as the AC offset becomes larger, the symmetric-chord damping is increased more than the symmetric-beam damping; eventually the chord damping exceeds the beam damping, but this effect is usually hidden by the limits imposed by antisymmetric modes. A parallel effect was seen in Fig. 9 for CG offsets, as discussed above for Fig. 7.

Detailed Examples

Three example rotors were chosen for closer study:
Rotor 1: 25% AC offset at blade segment #2
Rotor 2: 10% AC offset at blade segment #4
Rotor 3: 15% CG offset at blade segment #4

For reasons discussed above, 400 knots was the limit of the analysis, hence a 125-knot increase of the stability boundary was the maximum considered. Even a 100-knot increase puts the rotor far beyond its design operating point and is more than enough to illustrate the relative effectiveness of AC and CG offsets. Therefore, 100 knots was chosen as the criteria for selecting the examples below.

The most inboard location for which a 100-knot increase was seen for any AC variation was that of example rotor 1. The smallest AC offset giving a 100-knot benefit was that of example rotor 2 (Fig. 6). The maximum increase for any CG variation was 55 knots. The minimum CG offset needed to achieve this improvement was that of example rotor 3 (Fig. 7). Stability predictions for rotors 1, 2 and 3 are plotted in Figs. 10, 11 and 12, respectively; all predictions are based on the thin-wing airframe model.

Figure 10 shows the effects of 25% AC offset at blade segment #2 (rotor 1); the damping values for this rotor are plotted against those for the reference rotor. The symmetric chord (Fig. 10a) and anti-symmetric beam (Fig. 10b) modes are the most dramatically affected. These are the two modes with the lowest stability speeds for the reference rotor, so increasing their damping would have the largest effect on overall stability. Note that no modes at all go unstable for the modified rotor, and only the symmetric-beam mode would appear to eventually become unstable at some point beyond 400 knots.

Figure 11 shows the effects of 10% AC offset at blade segment #4 (rotor 2). Again, the symmetric-chord (Fig. 11a) and antisymmetric-beam (Fig. 11b) damping are the most changed. For this modified rotor, the symmetric-beam mode is unstable beyond 380 knots.

Figure 12 shows the effects of 15% CG offset at blade segment #4 (rotor 3). Yet again, the symmetric-chord (Fig. 12a) and antisymmetric-beam (Fig. 12b) modes are the most changed. The symmetric-beam

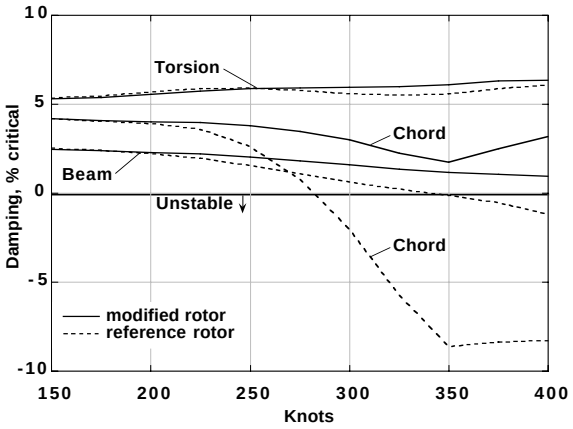

Fig. 10a. Symmetric whirl-mode damping versus airspeed for 25% AC offset at blade segment #2.

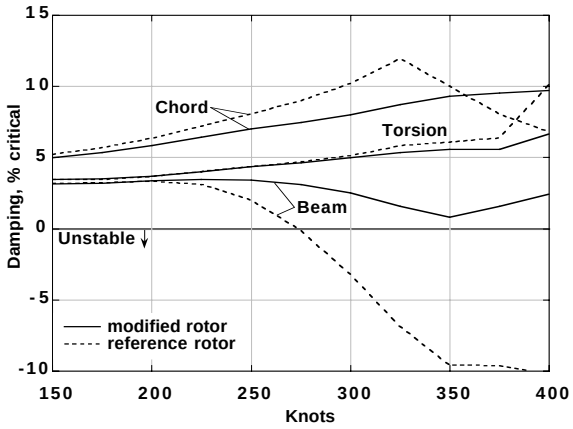

Fig. 10b. Antisymmetric whirl-mode damping versus airspeed for 25% AC offset at blade segment #2.

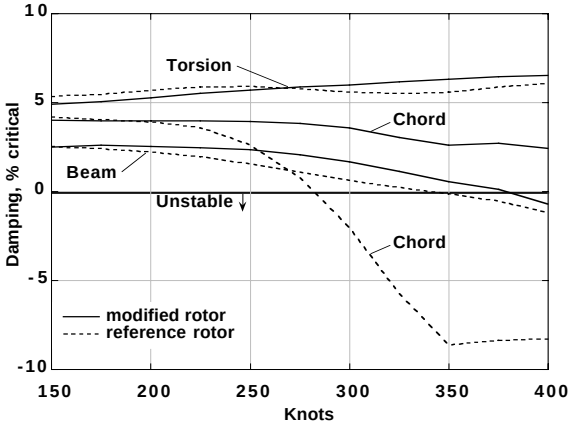

Fig. 11a. Symmetric whirl-mode damping versus airspeed for 10% AC offset at blade segment #4.

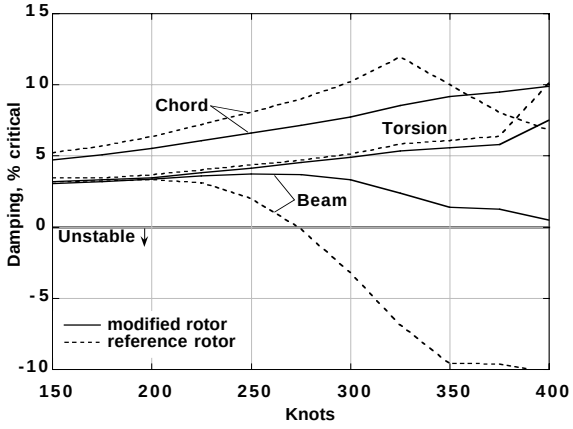

Fig. 11b. Antisymmetric whirl-mode damping versus airspeed for 10% AC offset at blade segment #4.

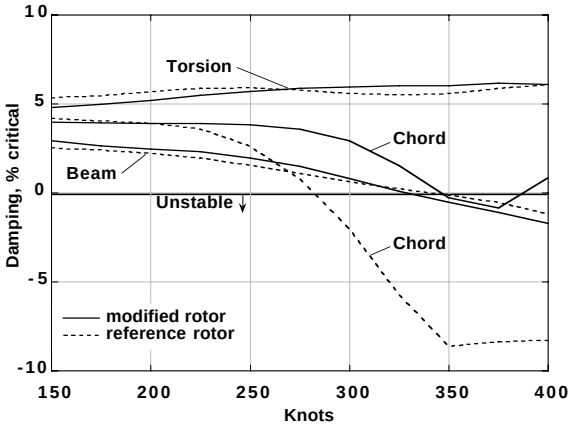

Fig. 12a. Symmetric whirl-mode damping versus airspeed for 15% CG offset at blade segment #4.

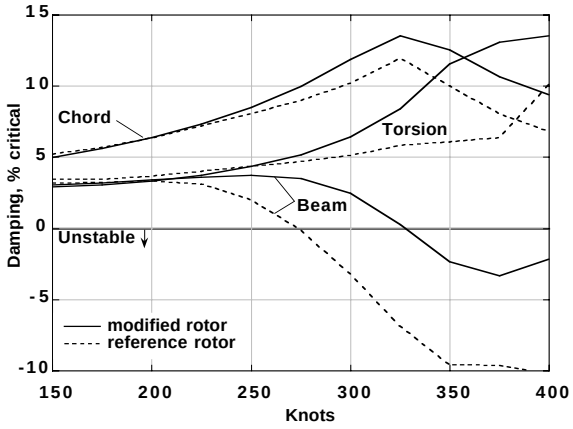

Fig. 12b. Antisymmetric whirl-mode damping versus airspeed for 15% CG offset at blade segment #4.

damping is almost unchanged, but it is only barely less stable than symmetric chord (Fig. 12a). With aerodynamic damping, symmetric beam would probably be more stable than symmetric chord. Antisymmetric torsion is also strongly affected (Fig. 12b), but as it is already heavily damped, the improvement is of comparatively little significance.

In all three examples, the modifications made the greatest improvements in the lowest-damped modes — symmetric chord and antisymmetric beam — with no significant reduction in the damping of the other modes. Note that because of the gradual slope of symmetric-beam damping, a small change to its damping would cause a large charge in its stability speed. However, the CAMRAD II model did not include aerodynamic damping, which would be expected to improve the stability of the symmetric-beam mode.

Loads Implications

The three example rotors were examined further to determine the effects of the parametric variations on rotor loads. Two flight conditions were analyzed:

1. Airplane mode at 250 knots, 458 rpm ($\mu = 0.70$), rotor $C_T/\sigma = 0.027$.
2. Helicopter mode (nacelle angle = 75 deg) at 80 knots, 565 rpm ($\mu = 0.18$), rotor $C_T/\sigma = 0.088$.

The airplane mode condition was chosen to ensure that the loads were calculated within the thin-wing stability boundary (Fig. 5) to provide a valid baseline reference.

Mean and 1/2 peak-to-peak oscillatory loads were calculated and plotted in Figs. 13 and 14. The figures include flap and lag bending moments at 0.35 *R* and pitch link force, all normalized to the reference (unmodified) rotor with the thin wing. Helicopter-mode loads are normalized to the helicopter reference, and airplane-mode loads are normalized to the airplane reference. Mean and oscillatory loads are plotted separately. The results for the three example rotors are plotted adjacent to each other for comparison, and airplane-mode results are plotted adjacent to helicopter-mode results for each type of load (lag, flap, and pitch-link loads).

All loads analyses included six harmonics of blade motion and 12 blade modes and were based on the thin-wing airframe model. In airplane mode, the analysis included wing/body interference velocities at the rotor. Uniform inflow was assumed because the differences caused by blade dynamics are of interest, for which momentum theory is adequate, especially in airplane mode. Development of a full wake model for helicopter flight was not justified at this stage of the research, which is focused on flutter, not loads. The objective of the loads analysis was to check for large adverse load variations.

Examination of Fig. 13 shows that none of the example variations had severely adverse effects on mean loads in airplane mode. However, rotor 1 (25% AC offset at blade segment #2) increased the pitch-link load by almost 70% in helicopter mode. Mean flap-bending loads were almost always reduced compared to the baseline rotor.

In Fig. 14, lag- and flap-bending oscillatory loads were little affected, but pitch-link loads were greatly increased in airplane mode for all example variations. In helicopter mode, rotor 1 had almost three times the oscillatory pitch-link load as the baseline rotor, whereas the other two example rotors had lower pitch-link loads than the baseline.

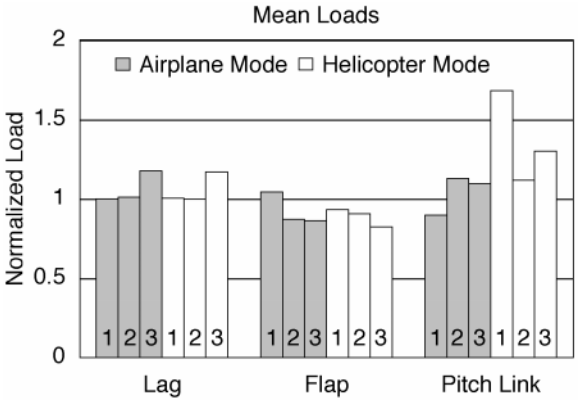

Fig. 13. Mean rotor loads, normalized to the baseline rotor, for rotor designs 1, 2, and 3.

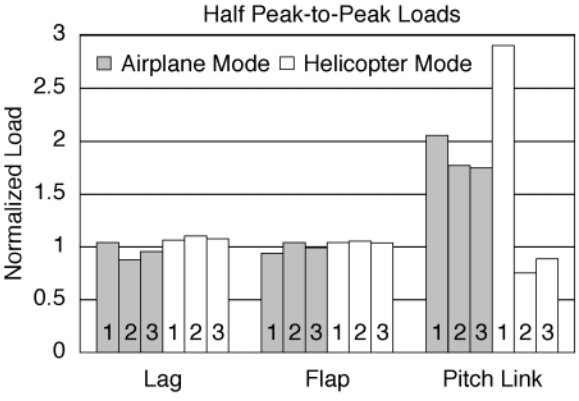

Fig. 14. Oscillatory rotor loads, normalized to the baseline rotor, for rotor designs 1, 2, and 3.

It is tempting to conclude that modifications to inboard blade segments cause worse loads than modifications to outboard segments, but the number of examples examined for loads was far too few to draw definitive conclusions. Furthermore, this was merely a preliminary analysis; an extensive loads-correlation effort would be necessary for definitive results. Nevertheless, the key result is that there exist combinations of parameters that give large increases in the whirl-mode stability boundary without excessive increases in loads.

Conclusions and Recommendations

The XV-15 rotor was analyzed with CAMRAD II to examine the effects on whirl-mode aeroelastic stability of chordwise offsets of the rotor blade aerodynamic center and center of gravity. The XV-15 model was modified to have a thinner wing (15% *t/c*) to better reveal the effects of the modifications. Small rearward offsets of the aerodynamic center created large increases in the stability boundary, in some cases by over 100 knots. The effect grew progressively stronger as the AC and CG offsets were shifted radially outboard. Forward offsets of the blade center of gravity had similar effects, but the maximum improvement seen was limited to 55 knots. For the range of offsets analyzed, CG offsets had a more linear effect on stability than AC offsets. Proper choice of parametric variations can avoid excessive increases in rotor loads. Limited-power trim proved slightly less stable than windmill-state trim.

These results can be applied to tiltrotors in several ways, most obviously to reduce the wing thickness for improved cruise performance while retaining adequate whirl-mode stability margins. In the present study, the wing thickness-to-chord ratio was reduced from 23% to 15% without decreasing the whirl-mode boundary. Thickness could in principle be retained while reducing weight or increasing aspect ratio, as appropriate for the performance goals of a particular design. Offsets of the blade aerodynamic center and center of gravity should be utilized as primary design variables because of their powerful effects on whirl-mode stability.

The present study analyzed a broad range of large offsets. Follow-on research should examine smaller increments of the key parameters, and should focus on the outboard blade segments, where the effect is largest. This would better define optimum values and sensitivities for more realistic design values. It would also be appropriate to examine the effects for a rotor explicitly designed for very high speeds, with re-optimized twist, airfoil sections, taper, etc. The analysis could be usefully extended to more radical blade concepts, such as inverse-taper and external mass booms, and to examine the interplay between blade design parameters and control system stiffness, delta-3, and other variables.

Appendix: XV-15 Tiltrotor Finite Element Stick Model

Introduction

This appendix describes the tiltrotor finite element stick models used in the aeroelastic stability predictions presented in this paper. The models are based on the Bell XV-15 tiltrotor structural characteristics. The “thick wing” model consists of an elastic wing with 23% thickness to chord ratio (*t/c*). The model uses one-dimensional elements exclusively, hence the name “stick” model. The normal modes of this stick model are calculated using MSC NASTRAN for Windows (Ref. 13). A CAMRAD II (Ref. 9) aeroelastic stability analysis is performed using the stick model mode shapes, frequencies and modal masses as input data. The stick model CAMRAD II stability results are compared with CAMRAD II stability results using frequencies and mode shapes from a detailed NASTRAN structural model of the XV-15 (Ref. 15). There is good agreement between the CAMRAD II stick model aeroelastic stability results and the CAMRAD II detailed NASTRAN model aeroelastic stability results.

The stick model structural properties are revised to represent an XV-15 tiltrotor with a 15% *t/c* composite wing. The mode shapes, frequencies, and modal masses of this model are used to create a CAMRAD II aeroelastic stability model of an XV-15 with a 15% *t/c* wing. This “thin wing” CAMRAD II model is used to assess the effect of proprotor design parameters on aeroelastic stability as presented in the body of this report.

Finite Element Stick Model Development

The finite element stick model is developed using the XV-15 finite element stick model by Wolkovitch et al. (Ref. 16) as a starting point. The model is based on the XV-15 geometry (Fig. 2, Ref. 12), weights

(Ref. 17), and wing structural characteristics (Ref. 15). The model consists of a 10-element elastic wing with a rigid fuselage and rigid wing-tip mounted nacelles (Fig. 15). Two concentrated masses model the left and right rotors and hubs. The following are additions to the Wolkovitch model to more closely model the actual XV-15 airframe structural characteristics:

1. The wing is assumed rigid in torsion and chord bending between the wing-to-fuselage mounting points at butt-line of 28 and –28 inches (the wing is assumed elastic in beam bending between the wing-to-fuselage mounting points). This is done to account for the high stiffness at the mounting points created by the fuselage structure.

2. The fuselage and nacelle elements are offset below the plane of the wing. This lowers the fuselage and nacelle centers of gravity relative to the wing. The fuselage and nacelle node points remain in the plane of the wing, the same as the Wolkovitch model.

3. A roll inertia element is added to the fuselage. The inertia of this element is adjusted to lower the wing antisymmetric beam bending mode frequency to match the detailed NASTRAN model antisymmetric beam bending frequency.

The thick wing stick model characteristics are summarized in Table 1. The stick model geometry is compared with the XV-15 detailed NASTRAN geometry in Fig. 15 and 16.

Zero Airspeed Mode Shapes and Frequencies

The six lowest frequency airframe modes are calculated by NASTRAN for Windows and input into CAMRAD II. These modes correspond to three symmetric wing modes and three antisymmetric wing modes and are critical for whirl flutter. The mode shapes calculated by NASTRAN are shown in Fig. 17. Notice that the airframe mode shapes are highly coupled and hence the mode titles are somewhat arbitrary. For example, the antisymmetric beam mode has a large component of wing torsion as well as beam bending.

Tables 2-4 present the modal data for the NASTRAN models used in this study. The mode frequency, mass, displacements, and rotations at the right rotor hub are shown for the stick model in Table 2. The corresponding detailed NASTRAN model data are shown in Table 3, and the data for the 15% *t/c* wing are shown in Table 4.

Stick Model Stability Results

The CAMRAD II aeroelastic stability analysis is performed with limited-power trim criteria (level flight up to maximum power, constant power thereafter). The rotor is trimmed to 457 rpm at sea-level standard conditions. The CAMRAD II stability results using the stick model airframe modes for the thick wing are plotted in Figs. 18 and 19. For comparison, stability results using the detailed NASTRAN airframe model modes are also plotted in Figs. 18 and 19. The stick model results are very similar to the detailed model results. The frequency and damping curves demonstrate similar characteristics.

CAMRAD II predicts a 24-knot higher symmetric chord mode instability speed for the stick model than for the detailed model. The stick model yields an 11-knot higher antisymmetric beam mode instability

Table 1. XV-15 finite element stick model characteristics.

Component	Element Type	Number of Elements	Length, ft	Weight, lb
Wing[a]	Elastic Beam	10	32.4	2,534
Left and Right Nacelle	Rigid Beam	4	7.7	3,166
Left and Right Rotor	Concentrated Mass	2	0	1,118
Fuselage[b]	Rigid Beam	2	42.1	6,182
	Concentrated Roll Inertia (4833 slug-ft^2)	1	0	0
			Gross Weight:	**13,000**

a. includes fuel, cross shafting, etc.

b. includes equipment, crew, and payload

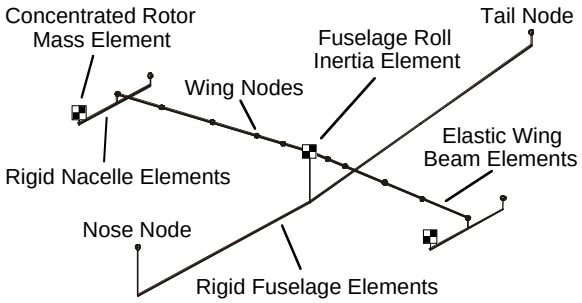

Fig. 15. XV-15 finite element stick model.

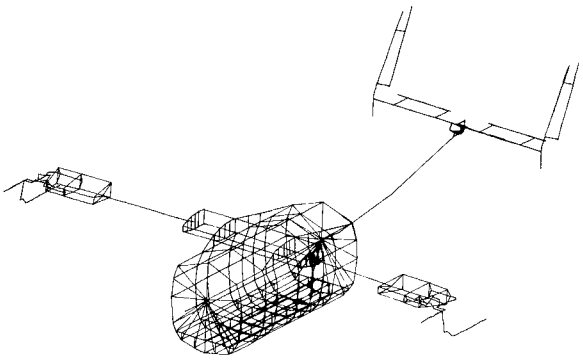

Fig. 16. XV-15 detailed finite element model from Ref. 15.

Symmetric beam mode (3.3 Hz)

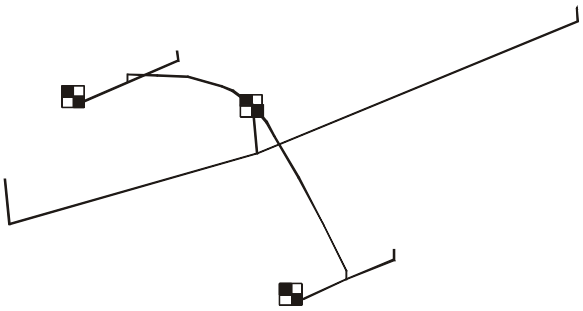

Antisymmetric beam mode (6.3 Hz)

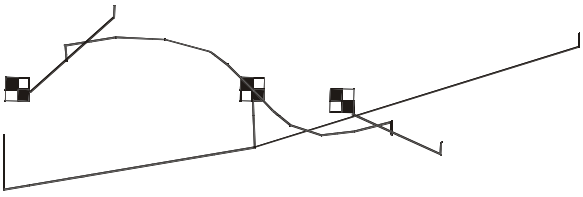

Symmetric chord mode (6.3 Hz)

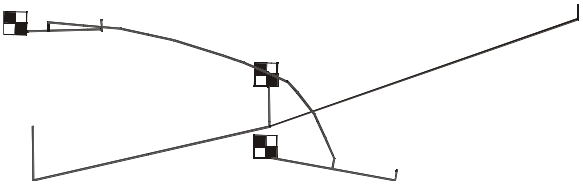

Antisymmetric chord mode (8.7 Hz)

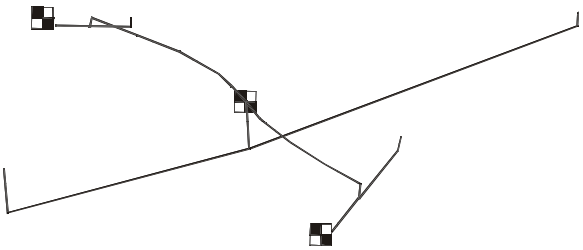

Symmetric torsion mode (8.3 Hz)

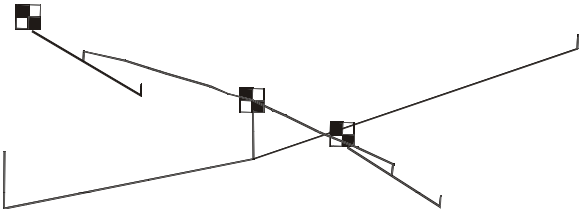

Antisymmetric torsion mode (7.1 Hz)

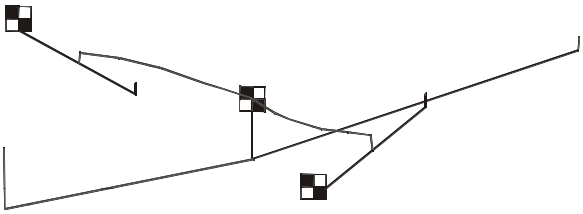

Fig. 17. XV-15 stick model mode shapes and frequencies (23% thick wing).

Table 2. Mode shapes at right hub for XV-15 finite element stick model (23% thick wing).

Mode Number	1	2	3	4	5	6
Sym. or Asy.	Sym.	Sym.	Sym.	Asy.	Asy.	Asy.
Mode Name	Beam	Chord	Torsion	Beam	Chord	Torsion
Frequency, Hz	3.3	6.3	8.3	6.3	8.7	7.1
Modal Mass, slugs	201.6	320.0	50.1	231.6	57.8	243.0
Structural Damping	0.03	0.07	0.08	0.05	0.05	0.06
Mode Shape:						
Displacement, ft						
X	-0.0275	1.0000	-0.1840	0.2702	-0.2500	0.7077
Y	0.0642	-0.9283	0.1235	-0.3044	0.0802	-0.3986
Z	1.0000	-0.2755	-0.5525	0.9438	-0.4516	-0.5767
Rotation, rad						
X	0.1385	0.0322	0.0405	0.1000	0.0651	0.0212
Y	-0.0251	0.1125	0.2027	-0.1561	0.1895	0.1951
Z	0.0025	-0.1903	0.0219	-0.0304	0.0308	-0.1244

Table 3. Mode shapes at right hub for XV-15 detailed finite element model (23% thick wing).

Mode Number	1	2	3	4	5	6
Sym. or Asy.	Sym.	Sym.	Sym.	Asy.	Asy.	Asy.
Mode Name	Beam	Chord	Torsion	Beam	Chord	Torsion
Frequency, Hz	3.4	6.6	8.2	6.3	7.9	7.7
Modal Mass, slugs	241.6	517.8	7.6	242.7	407.3	113.0
Structural Damping	0.03	0.07	0.08	0.05	0.05	0.06
Mode Shape:						
Displacement, ft						
X	-0.0014	-1.0000	-0.1142	-0.1329	-0.7699	-0.0763
Y	-0.0330	1.0311	0.0992	0.5231	0.3645	-0.1035
Z	-1.0000	1.1197	-0.2413	-0.8419	-0.5238	-0.9917
Rotation, rad						
X	-0.1463	-0.0698	0.0056	-0.1777	0.1012	0.0564
Y	0.0281	-0.3719	0.0800	0.1648	0.1914	0.3356
Z	0.0022	0.2615	0.0263	0.0384	0.1780	-0.0227

Table 4. Mode shapes at right hub for tiltrotor with conceptual 15% *t/c* wing.

Mode Number	1	2	3	4	5	6
Sym. or Asy.	Sym.	Sym.	Sym.	Asy.	Asy.	Asy.
Mode Name	Beam	Chord	Torsion	Beam	Chord	Torsion
Frequency, Hz	2.4	5.1	6.0	4.6	6.5	5.5
Modal Mass, slugs	194.8	154.6	66.5	199.1	117.1	86.6
Structural Damping	0.03	0.07	0.08	0.05	0.05	0.06
Mode Shape:						
Displacement, ft						
X	-0.0247	0.5407	-0.3597	0.1529	0.5504	-0.2675
Y	0.0620	-0.5340	0.2820	-0.2239	-0.2319	0.2010
Z	1.0000	-0.5074	-0.5447	1.0000	0.4176	0.4311
Rotation, rad						
X	0.1362	0.0481	0.0407	0.0796	-0.0754	-0.0594
Y	-0.0289	0.1968	0.2017	-0.1953	-0.1851	-0.1869
Z	0.0022	-0.1117	0.0540	-0.0095	-0.0791	0.0522

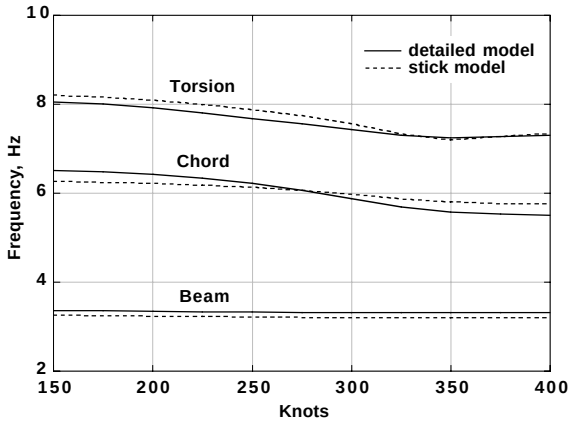

Fig. 18a. Frequency versus flight speed for XV-15 (symmetric wing modes).

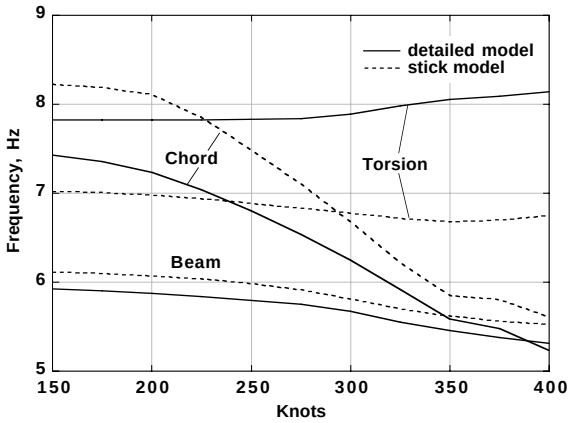

Fig.18b. Frequency versus flight speed for XV-15 (antisymmetric wing modes).

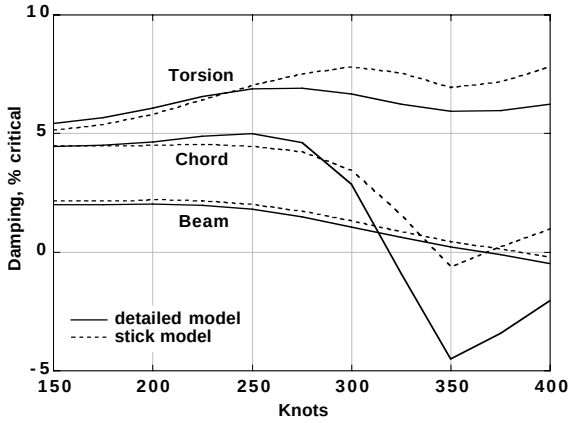

Fig. 19a. Damping versus flight speed for XV-15 (symmetric wing modes).

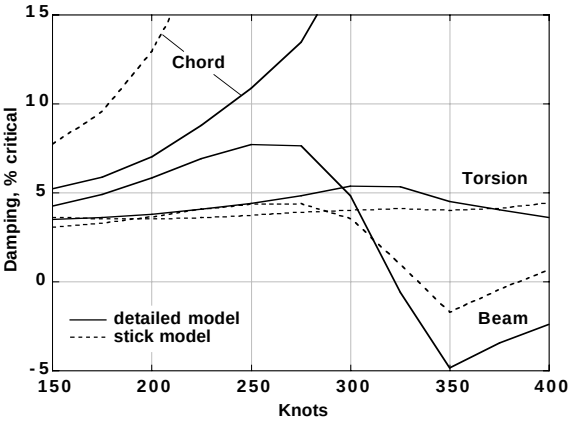

Fig. 19b. Damping versus flight speed for XV-15 (antisymmetric wing modes).

speed than the detailed model. The stick model frequencies closely match the detailed model except for the antisymmetric chord mode and antisymmetric torsion modes. For example, the stick model overpredicts the antisymmetric chord mode frequency by 0.4 Hz and underpredicts the antisymmetric torsion mode frequency by 1.1 Hz compared to the detailed model at 300 knots airspeed. The results indicate that the simple finite element stick model can be a useful substitute to a detailed finite element model for predicting the aeroelastic stability of low frequency airframe modes.

15% *t/c* Wing Characteristics

To evaluate proprotor design options for improving whirl-flutter stability, a notional XV-15 with a 15% *t/c* graphite epoxy wing is conceptually defined. The wing is assumed to have the same geometry as the XV-15 wing except for reduced thickness. The 15% *t/c* wing structure is sized based on static strength (2g jump take-off and 4g pull-up) and static divergence (529 knots at sea-level standard conditions). The wing structure is not sized to meet a minimum whirl-flutter speed requirement. The wing structural characteristics are estimated using the methods presented in Ref. 18. These methods are appropriate for estimating tiltrotor wing strength, stiffness, and weight at a conceptual design level. The design characteristics of the 15% *t/c* wing are compared with the original XV-15 in Table 5.

Stability of Stick Model with 15% *t/c* wing

The 15% *t/c* wing stiffness and mass characteristics are input into the MSC NASTRAN for Windows XV-15 stick model. The mode frequencies and shapes of the 15% *t/c* wing model are listed in Table 4. CAMRAD II stability predictions for the XV-15 with the 15% *t/c* wing are shown in Figs. 4 and 5.

Table 5. Wing structural comparison.

	XV-15 wing (23% *t/c*)	Conceptual wing (15% *t/c*)
Weights		
Torque Box, lb	567	260
Spars, lb	52	34
Control Surfaces, lb	97	77
Fairings, lb	108	86
Fittings, other, lb	122	122
Total Wing, lb	946	579
Material Properties		
Material	Aluminum	Graphite Epoxy
Elastic Modulus, Torque Box, lb/in^2	10,000,000	9,000,000
Elastic Modulus, Spars, lb/in^2	10,000,000	18,000,000
Shear Modulus, Torque Box, lb/in^2	3,800,000	3,750,000
Density, lb/in^3	0.1	0.06
Limit Strain, in/in	0.0068	0.0047
Wing Stiffness		
Beam Bending, lb-in^2	3.70E+09	1.98E+09
Chord Bending, lb-in^2	1.12E+10	7.59E+09
Torsion, lb-in^2	2.80E+09	1.33E+09

The aeroelastic instability speed is reduced from 335 knots (antisymmetric beam mode) for the XV-15 with 23% *t/c* wing to 275 knots (antisymmetric beam mode) for the XV-15 with the conceptual 15% *t/c* wing. The CAMRAD II model of the XV-15 with 15% *t/c* wing serves as the baseline for evaluating proprotor design options for improving whirl-flutter stability as presented in the main report.

Acknowledgments

The authors wish to thank Franklin D. Harris for his suggestions for the table-top model and for his constructive criticisms and enthusiastic support of the research. The authors also wish to thank John F. Madden, whose insight led to the aerodynamic-offset analyses and whose continuing suggestions have strongly influenced the research effort.

References

1. Corso, L. M., Popelka, D. A., and Nixon, M. W., "Design, Analysis, and Test of a Composite Tailored Tiltrotor Wing," American Helicopter Society 53rd Annual Forum, Virginia Beach, Virginia, April 29-May 1, 1997.

2. Popelka, D., Lindsay, D., Parham, T., and Berry, V., "Results of an Aeroelastic Tailoring Study for a Composite Tiltrotor Wing," American Helicopter Society 51st Annual Forum, Fort Worth, Texas, May 9-11, 1995.

3. Nixon, M. W., "Parametric Studies for Tiltrotor Aeroelastic Stability in High Speed Flight," *Journal of the American Helicoter Society*, Vol. 38, No. 4, October 1993.

4. van Aken, Johannes M., "Alleviation of Whirl-Flutter on Tilt-Rotor Aircraft Using Active Controls," American Helicopter Society 47th Annual Forum, Phoenix, Arizona, May 6-8, 1991.

5. Matuska, D. G., and Studebaker, K., "Reduced Tip Speed Testing of a Variable Diameter Tiltrotor," European Rotorcraft Forum, Italy, September 1993

6. Srinivas, V., Chopra, I., and Nixon, M. W., "Aeroelastic Analysis of Advanced Geometry Tiltrotor Aircraft," *Journal of the American Helicoter Society*, Vol. 43, No. 3, July 1998.

7. Detore, J. A., and Gaffey, T. M., "The Stopped-Rotor Variant of the Proprotor VTOL Aircraft," *Journal of the American Helicoter Society*, Vol. 15, No. 3, July 1970.

8. Madden, J. F. III, and Peyran, R. J., "Aeroelastic Stability Enhancer for Tilt-Rotor Aircraft," Invention Disclosure, NASA Case No. ARC-14298-1CU, May 1998.

9. Johnson, W., “CAMRAD II Comprehensive Analytical Model of Rotorcraft Aerodynamics and Dynamics — Theory Manual,” Johnson Aeronautics, Palo Alto, California, 1993.

10. Johnson, W., Lau, B. H., and Bowles, J. V., “Calculated Performance, Stability, and Maneuverability of High Speed Tilting Proprotor Aircraft,” 12th European Rotorcraft Forum, Garmisch-Partenkirchen, Germany, September 22-25, 1986.

11. Johnson, W., “CAMRAD II Comprehensive Analytical Model of Rotorcraft Aerodynamics and Dynamics — Rotorcraft Applications,” Johnson Aeronautics, Palo Alto, California, 1993.

12. Maisel, M., “Tilt Rotor Research Aircraft Familiarization Document,” NASA TN X-62, 407, January 1975.

13. MacNeal-Schwendler Corporation, “MSC NASTRAN for Windows — Evaluation Guide and User’s Manual,” MSC Inc., Los Angeles, California, 1997.

14. Staff of Bell Helicopter Company, “Advancement of Proprotor Technology. Task II — Wind-Tunnel Test Results.” Bell Helicopter Company Report 300-099-004, NASA CR-114363, September 1971.

15. Staff of Bell Helicopter Company, “V/STOL Tilt Rotor Research Aircraft — Volume 3: Structural Loads and Dynamics,” Bell Helicopter Co. Report No. 301-199-003, 1974.

16. Wolkovitch, J., Wainfan, B., Ben-Harush, Y., and Johnson, W., “Application of the Joined Wing to Tiltrotor Aircraft,” NASA CR-177543, November 1989.

17. Arrington, W., Kumpel, M., Marr, R., and McEntire, K., “XV-15 Tilt Rotor Research Aircraft Flight Test Data Report,” NASA CR-177406, June 1985.

18. Chappell, D. P., and Peyran, R. J., “Methodology for Estimating Wing Weights for Conceptual Tilt Rotor and Tilt Wing Aircraft,” Society of Allied Weight Engineers 51st Annual Conference, Hartford, Connecticut, May 1992.